REGIONAL AND GLOBAL DUST STORMS ON MARS INVESTIGATED US-ING DATA ASSIMILATION.

T. Ruan, R. M. B. Young, P. L. Read, *Atmospheric, Oceanic and Planetary Physics, Department of Physics, University of Oxford, Clarendon Laboratory, Parks Road, Oxford, OX1 3PU, UK (roland.young@physics.ox.ac.uk),* **S. R. Lewis,** *School of Physical Sciences, The Open University, Walton Hall, Milton Keynes, MK7 6AA, UK,* **L. Montabone,** *Atmospheric, Oceanic and Planetary Physics, Department of Physics, University of Oxford, Clarendon Laboratory, Parks Road, Oxford, OX1 3PU, UK, Space Science Institute, Boulder, CO 80301, USA.*

Introduction

The dust cycle is a key component of the Martian climate, and its full understanding is extremely important for understanding the evolution of the Martian environment. Dust particles injected into the atmosphere greatly affect the dynamical and thermal state of the Martian atmosphere via its general circulation.

Intensive measurements of atmospheric temperature and dust extending over nearly ten Mars Years (MY) now exist with unprecedented spatial coverage, thanks to various orbital spacecraft including Mars Global Surveyor (MGS, 1997-2006), Mars Odyssey (MO, 2001-present), and Mars Reconnaissance Orbiter (MRO, 2006-present). Such observations have already helped to improve our understanding of Mars' weather and climate, but their incomplete coverage of the planet restrains our ability to study the general circulation in full detail. On the other hand, numerical models provide four-dimensional simulated data with high temporal and spatial resolution, but often fail to produce the dust cycle's realistic variability.

To aid this approach, data assimilation provides a solution that is consistent with both observations and modelled physical constraints. It corrects model-predicted variables towards observations such that the resulting solution can represent the full observed variability of the climate. This approach has been widely used as an effective tool in operational weather forecasting systems or climate models for analyzing meteorological variables for the Earth[1,2].

Lewis & Read[3] implemented the analysis correction (AC) scheme[1] in a simple version of a Mars General Circulation Model (MGCM) in order to assimilate temperature profiles from the Pressure Modulator Infrared Radiometer (PMIRR) instrument on-board the Mars Observer spacecraft (1993). Their results showed that assimilation of such observations was feasible and that it improved the agreement between model and observations. Lewis et al.[4] extended this approach to include dust tracer assimilation, which was combined with a full MGCM to assimilate thermal profiles and Column-Integrated Dust Opacity (CIDO) rescaled to a reference level (τ_{ref}) using retrievals from the Thermal Emission Spectrometer (TES) on-board MGS[5]. More recently, a complementary approach has been developed[6,7] using the ensemble Kalman filter[8], which was used to as-similate TES temperature retrievals; MCS temperature observations were later assimilated using this scheme[9].

Lewis et al.[4] and later studies[10–12] assimilated TES temperature profiles and τ_{ref} without explicitly advecting the dust tracer field, using an empirical relation[13] to prescribe the vertical distribution of dust. A more recent dataset from MCS on board MRO[14] provides vertically resolved, global measurements of the atmospheric dust distribution. With this in hand, here we use an updated dust data assimilation system that advects the dust and assimilates both CIDO and Layer-Integrated Dust Opacity (LIDO) observations to better represent the Martian dust cycle. We apply it to a southward-moving regional dust storm during MY29 and to the MY28 global dust storm (GDS).

Model and data assimilation

We use the UK version of a three-dimensional Martian Global Climate Model (UK-LMD MGCM)[15]. The model combines a spectral dynamical solver at triangular truncation T31, corresponding to a 96×48 longitude-latitude grid in real space, a tracer transport scheme and dust lifting routines, along with a full range of physical parameterizations.

The equations for a hydrostatic, adiabatic and inviscid gas surrounding a rotating spherical planet are cast in vorticity-divergence form. In the vertical, levels are defined in terms of the terrain-following σ coordinate system using a standard finite difference approach. There are 25 levels with the first three at 4, 19, and 44 m above the surface, to resolve detailed surface processes represented in the model. The model top varies over time but is typically around 100 km, with a sponge layer (linear drag on eddy vorticity and divergence) in the uppermost three level to reduce spurious reflection of vertically propagating waves. There are 480 dynamical and 96 physics timesteps per sol.

The radiative transfer scheme calculates atmospheric absorption and emission due to carbon dioxide and airborne dust; water's radiative effects are not included. The balance between incoming radiative flux and thermal conduction in the soil contributes to changes in surface temperature, using a surface thermal inertia field derived from TES and Viking measurements[15] and topog-

raphy from the Mars Orbiter Laser Altimeter (MOLA) on MGS[16]. The surface roughness length z_0 is based on a global map compiled by Hébrard et al.[17], and implemented in the UK-MGCM by Mulholland[18].

The dust transport scheme includes a dust lifting scheme, tracer advection, gravitational sedimentation and deposition. We use a $1.5\,\mu m$ particle size based on Mars Exploration Rover observations[19]. The two most important distinct mechanisms responsible for the injection of dust into atmosphere are thought to be dust lifting by near-surface wind stress, and dust lifting by dust devils[20].
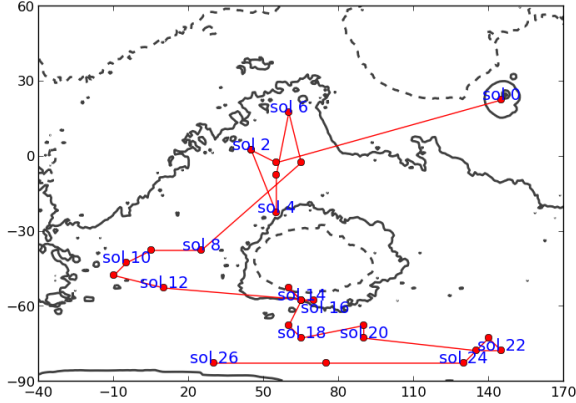

Figure 1: The route followed by the centre of the regional dust storm. Sols are relative to the beginning of the storm period.

The data assimilation scheme is based on the Analysis Correction sequential estimation (AC) scheme[1] but with modifications specific to Mars[4]. The assimilation step is computationally inexpensive compared with the rest of the model, and so is performed at each dynamical timestep. Lewis et al.[4] describe the scheme in full detail. Temperature assimilations are the same, but use TES data. We have extended the dust assimilation to use active dust transport, and assimilate both CIDO and LIDO, simultaneously where possible.

Observational datasets

Measurements of atmospheric temperature and dust now exist covering the Martian atmosphere over nearly eight MYs. The instruments for measuring temperature and dust on board these spacecraft are TES on MGS[21], THEMIS on MO[22] and MCS on MRO[14].

TES and THEMIS dust retrievals contain CIDO data, while MCS contains the most up-to-date satellite observations with vertically resolved, simultaneous global measurements of atmospheric temperature, LIDO, and water[23]. This contains information on the day-to-day variability of Martian weather from the near surface to the top of the middle atmosphere around $80\,km$ altitude[14]. The spacecraft have different operational periods and or-

bits, so their retrievals have different temporal and spatial coverage. Only THEMIS has overlapping observational periods with the other two datasets. Further details of the THEMIS dataset, including the retrieval algorithm, can be found in Smith et al.[5],[24] and Smith[22].

Upward-looking surface observations provide a view of CIDO that is independent of satellite-based datasets, although only over a limited area. The MER missions Spirit ($14.57\,°S$, $175.48\,°E$) and Opportunity ($1.95\,°S$, $5.53\,°W$) provide almost continuous data coverage during MY28 and MY29. Both rovers carried a Pancam camera, which included solar filters at $440\,nm$ and $880\,nm$ wavelengths.
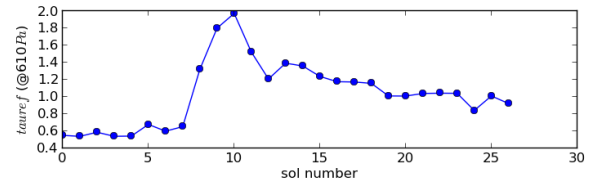

Figure 2: Peak dust opacity τ_{ref} at the storm center.

MY29 southward-moving regional dust storm

A dust storm was reported for more than 20 sols in weekly MRO MARCI (Mars Color Imager) Weather Reports (MMWR)[25]. The storm formed in the northern hemisphere over Utopia and western Elysium on MY29, $L_s \approx 305.2°$, moved southward along the Utopia storm track through Isidis and crossed the equator into Hellas, strengthened with additional dust lifting between Hellas and Noachis, moved westward through Noachis, halted but continued to spread dust over Noachis, Hellas, Promethei and part of Cimmeria, and decayed around MY29, $L_s \approx 313.9°$.

This event is interesting because the dust cloud associated with this storm appeared to travel through one of the important channels connecting the Northern and Southern hemisphere (Utopia-Isidis), the duration of this storm duration was quite long, and the THEMIS and MCS datasets provide excellent coverage in this area during this period.

CIDO and LIDO retrievals from THEMIS and MCS respectively were assimilated into the model over this period. Every 10th THEMIS data point and every 10th MCS vertical profile was not assimilated, but retained for out-of-sample verification.

One advantage of using data assimilation is that it is possible to track the route of a migrating dust storm in a way that is not possible using observations alone. We assumed the the dust storm to be rectangular, initially $11.25°\times11.25°$ during formation over Elysium, increasing to $33.75°\times33.75°$ as it moved south. The rectangle with the highest average τ_{ref} defined the location of the storm, and the grid cell with the highest τ_{ref} within that

rectangle defined its centre. Figure 1 shows the location of the storm centre tracked in this way. It is possible that the changing location of the dust storm is due to a sequence of discrete lifting events rather than the physical movement of the storm as a coherent system, but this remains an open question about Mars' dust cycle and the evolution of individual events.
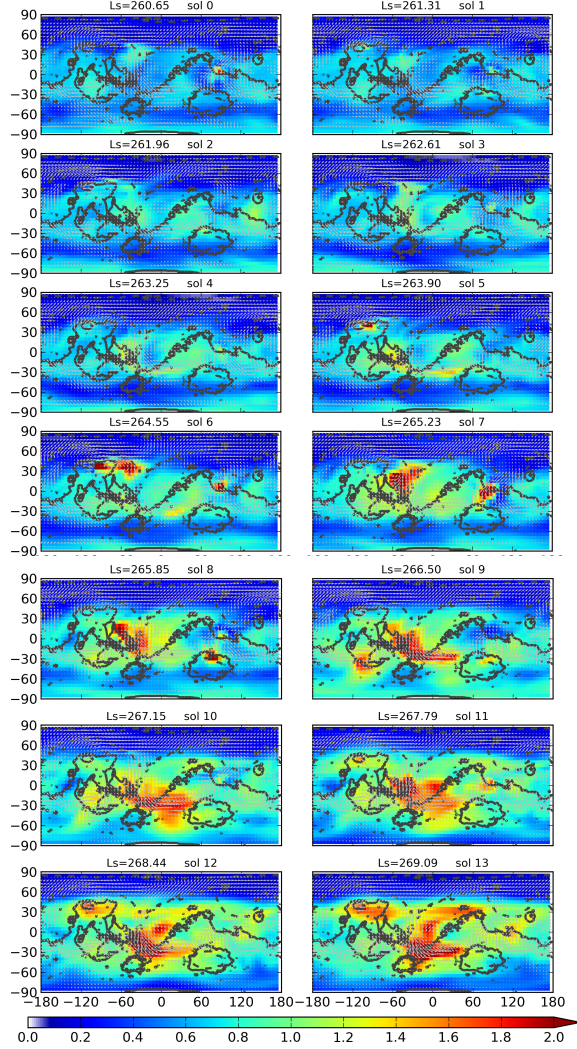
Data assimilation was also able to reveal how high the dust cloud penetrated during the evolution of this storm. Before this storm, dust layer tops were normally seen to reach to heights of $\sim 12\,\mathrm{km}$, but the reanalysis showed that this storm transported dust as high as $\sim 30\,\mathrm{km}$.
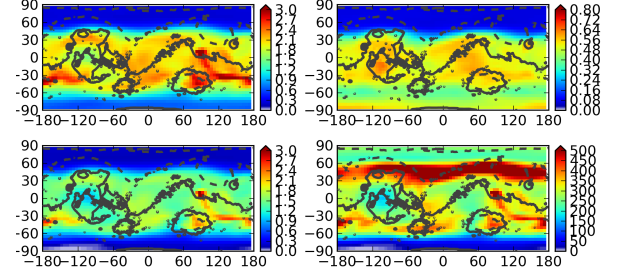

Figure 4: τ_{ref} averaged over the MY28 GDS period ($L_s \approx 269.1° \sim 309.5°$, top left), averaged over the same L_s range during MY29 (top right), and their absolute (bottom left) and percentage (bottom right) differences.

MY28 global dust storm

During MY28 a precursory dust storm travelled southwards from Chryse, originating on $L_s \approx 261°$. After five sols, dust clouds were observed near Noachis, where the storm grew significantly in scale and intensity, developing into a planet-encircling storm soon afterwards[26]. However, Wang & Richardson[26] were unable to unambiguously establish a clear relationship between the precursor dust storm from Chryse Planitia, dust events in Noachis, and what actually led to the initiation of the MY28 GDS. We have used assimilation to investigate the evolution of the MY28 GDS and its effect on the wider circulation.

During this period THEMIS CIDO retrievals were quite sparse, mainly covering the Southern Hemisphere. MCS provided more extratropical profiles, and a relatively even distribution globally, but almost no data to the south of $\sim 45°$ within $L_s \approx 270° \sim 295°$, covering most of the GDS period. This was compensated for by a high THEMIS data density in the Southern Hemisphere during that period. Both datasets were assimilated into the MGCM over the period of the GDS.

The assimilation showed that during the precursor event (Fig. 3), dust devil lifting appeared to provide the background dust level, mostly in the southern hemisphere. Dust lifted by wind stress was found to be more strongly correlated with various centres of dust activity during the same period. Wind stress dust lifting was important in Alba Patera, the Acidalia-Chryse channel, Xanthe Terra, Elysium Planitia, and Noachis Terra.

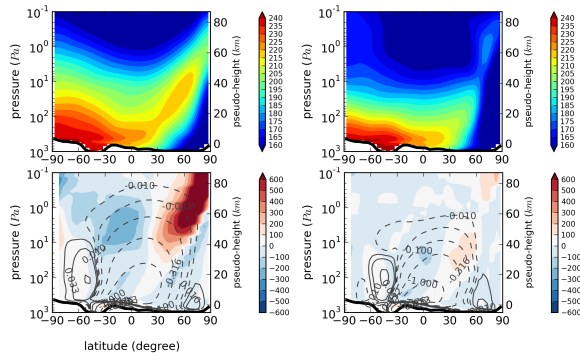To gauge the effect of the MY28 GDS on the wider circulation, we compared the analysis with an analysis

Figure 3: Reanalysis showing daily-averaged τ_{ref} during the precursor event leading up to the MY28 GDS. Sol 0 corresponds to $L_s \approx 260.7°$, when the dust storm was first reported in the MMWR. Arrows show the $4\,\mathrm{m}$ wind velocity.

The peak opacity at the storm centre can be seen in Fig. 2. In sols 0–5, the centre remained between Arabia and Hellas until the dust cloud formed a clear shape in sol 5. From sols 8–11, two separate centres combined and moved westward, with the storm reaching its maximum opacity during sol 10 (see Fig. 2). Once it arrived at its farthest westward point, the storm centre slowly decayed.

Figure 5: Top: Zonal-time mean temperature (K, top); Bottom: zonal-time mean mass stream function (10^{10} kg s^{-1}, contours) and adiabatic heating rate (K sol^{-1}, colour). Both are averaged over $L_s \approx 269.1° \sim 309.5°$ for MY28 (left) and MY29 (right). The black line shows the approximate zonal mean topography. Stream function contour intervals are logarithmic with negative values indicating clockwise circulation.

covering $L_s \approx 269.1° \sim 309.5°$ in the following MY29, which did not have a GDS. Figure 4 shows maps of τ_{ref} averaged over the MY28 GDS, compared with the same period in MY29, together with the differences between these two averages. The percentage difference suggests that the largest difference compared to MY29 was found between $30°$–$60°$ in the Northern Hemisphere, which corresponds to the boundary of the polar vortex. Although during the GDS the dust seemed was mostly confined to latitudes $60°$S and $45°$N, the percentage difference compared to MY29 was largest in the North Polar region. In contrast, the South Polar region had the lowest percentage differences compared to MY29.

Because of the thermal effects of suspended dust particles, temperature variations on Mars always show a strong correlation with the distribution of dust. Figure 5 (top) shows the zonal-time mean temperature during MY28 and MY29. The atmosphere during the MY28 GDS was warmer than during MY29, and the the vertical temperature gradient below 100 Pa over the South Pole was larger during MY29. During MY28 the polar warming in the Northern Hemisphere was very strong, with a deep vertical extension (~ 150 Pa — above 0.1 Pa). The more intensive heating is near the top of the dust storm, however, which reduces the incoming solar radiation intensity in the lower atmosphere, so the atmosphere near the ground was cooler during MY28.

Figure 5 (bottom) shows the zonally averaged stream function and adiabatic heating rate during the GDS time window. In the GDS year the meridional circulation was significantly strengthened, both vertically and poleward. The adiabatic heating rate in the North Polar region also increased significantly with a maximum value more than triple that during MY29.

Summary

We have updated the UK-MGCM dust data assimilation system to actively transport dust and simultaneously assimilate CIDO and LIDO observations. This was used to study a regional dust storm during MY29 and the MY28 global dust storm. The reanalyses reveal several features of the atmospheric circulation that cannot be deduced using the observations or model by themselves.

References

1 Lorenc, AC et al. 1991, QJRMS, 117, 59
2 Kalnay, E 2003, Atmospheric Modeling, Data Assimilation and Predictability (CUP)
3 Lewis, SR, & Read, PL 1995, ASR, 16, 9
4 Lewis, SR et al. 2007, Icarus, 192, 327
5 Smith, MD et al. 2003, JGR, 108, 5115
6 Hoffman, MJ et al. 2010, Icarus, 209, 470
7 Greybush, SJ et al. 2012, JGR, 117, E11008
8 Evensen, G 2003, Ocean Dyn., 53, 343
9 Navarro, T et al. 2014, GRL, 41, 6620
10 Wilson, RJ et al. 2008, GRL, 35, L07202
11 Rogberg, P et al. 2010, QJRMS, 136, 1614
12 Montabone, L et al. 2014, Geosci. Data J., 1, 129
13 Conrath, BJ 1975, Icarus, 24, 36
14 Kleinböhl, A et al. 2009, JGR, 114, E10006
15 Forget, F et al. 1999, JGR, 104, 24155
16 Smith, DE et al. 2001, JGR, 106, 23689
17 Hébrard, E et al. 2012, JGR, 117, E04008
18 Mulholland, DP 2012, DPhil thesis, University of Oxford
19 Lemmon, MT et al. 2004, Science, 306, 1753
20 Newman, CE et al. 2002, JGR, 107, 5123
21 Smith, MD 2004, Icarus, 167, 148
22 Smith, MD 2009, Icarus, 202, 444
23 McCleese, DJ et al. 2010, JGR, 115, E12016
24 Smith, MD et al. 2000, JGR, 105, 9539
25 Malin, MC et al. 2009, MRO MARCI Weather Reports for 13/7/2009–2/8/2009, Malin Space Science Systems Captioned Image Releases, MSSS-92,-93,-94, http://www.msss.com/msss_images/
26 Wang, H & Richardson, MI 2013, Icarus, 251, 112